

Buckling of residually stressed cylindrical tubes under compression

Tao Zhang^a, Luis Dorfmann^b, Yang Liu^{c,a,*}

^a*Department of Mechanics, School of Mechanical Engineering, Tianjin University, Tianjin 300350, China*

^b*Department of Civil and Environmental Engineering, Tufts University, Medford, MA, USA*

^c*Mathematical Institute, University of Oxford, Oxford, OX2 6GG, UK*

Abstract

We evaluate the loss of stability of axially compressed slender and thick-walled tubes subject to a residual stress distribution. The nonlinear theory of elasticity, when used to analyze the underlying deformation, shows that the residual stress induces preferred directions in the reference configuration. The incremental theory, given in Stroh form, is used to derive an exact bifurcation condition. The critical stretch and the associated critical buckling mode are identified for axisymmetric and asymmetric increments in the deformation. Mode transitions are illustrated as the tube slenderness varies. For slender tubes, Euler buckling is energetically favorable, and the effect of residual stress is negligible. However, for short and thick-walled tubes where barreling mode is dominant, the residual stress significantly affects the buckling behavior and may eliminate barreling instability. We show that, depending on its magnitude and direction, residual stress can either accelerate or delay instability. Phase diagrams for various modes are obtained and provide insight into pattern selection across different tube geometries.

Keywords: Buckling of tubes, Residual stress, Bifurcation analysis, Nonlinear elasticity, Stroh formalism

1. Introduction

Tubular structures are frequently encountered in both biology and engineering applications—for example, blood vessels (Fung, 1993; Sokolis, 2015), microtubules in cells (Brangwynne et al., 2006; Li, 2008), packers used in petroleum engineering (Liu, 2018; Lan et al., 2019), and cellular foams (Chawla et al., 2022), among others. In practice, these structures may undergo finite deformations, making them susceptible to buckling under combined axial and transverse loads. In a seminal study, Koiter (1945) developed a post-buckling theory and demonstrated that imperfection sensitivity can cause an axially compressed cylindrical shell to collapse earlier than theoretical prediction. Since then, the stability and bifurcation behavior of cylindrical tubes or shells under various load conditions have been a topic of fundamental interest in both the mechanics and engineering communities.

For thick and incompressible neo-Hookean tubes subjected to end loads, Wilkes (1955) employed finite deformation theory to investigate buckling instability. An important finding was that the associated eigenvalue problem arising from a linear bifurcation analysis in cylindrical polar coordinates can be solved exactly in terms of Bessel functions. Decades later, this classical problem was revisited by Pan and Beatty (1997a,b, 1999) and results for different material models were

*Corresponding author.

Email address: liuy3@maths.ox.ac.uk, tracy_liu@tju.edu.cn (Yang Liu)

provided. Considering material compressibility, Dorfmann and Haughton (2006) explored the full bifurcation landscape for tubes under axial compression and unveiled two distinct forms of the barreling mode. Goriely et al. (2008) re-derived the exact bifurcation condition for incompressible tubes of arbitrary wall thickness and length under compression using the Stroh formalism. They also obtained useful asymptotic solutions and constructed a phase diagram characterizing different bifurcation modes. Springhetti et al. (2023) re-established the classical conditions for thin-walled cylinders and proposed a generalized framework applicable to a broad class of nonlinear hyperelastic materials.

These studies focused on using the nonlinear theory to determine the critical buckling loads and corresponding mode shapes. However, they do not provide insight into the post-buckling evolution or the nature of the bifurcation. To address this gap, Dai et al. (2015) adopted a coupled series-asymptotic expansion to derive a reduced model applicable for thin-walled tubes. Focusing on asymmetric bifurcation modes, they obtained analytical post-buckling solutions and revealed the counterintuitive result that a thick-walled tube may be softer than a thin one. Recently, Zhou et al. (2023) performed a post-buckling analysis of axially compressed thick-walled tubes in a fully three-dimensional setting to highlight the influence of geometric parameters on both buckling and post-buckling behaviors.

In many practical applications, tubular structures are subjected to complex loading conditions. To advance the understanding of tube stability under such conditions, Haughton and Ogden (1979a,b) developed an analysis for both thin- and thick-walled tubes subjected to axial force and internal pressure. They examined prismatic, axisymmetric, and asymmetric buckling modes, and showed how geometric parameters, such as wall thickness, length-to-radius ratio, and axial stretch influence the onset of instability. Zhu et al. (2008) provided a comprehensive bifurcation analysis of thick-walled tubes under combined axial load and external pressure, capturing a rich spectrum of asymmetric and axisymmetric modes across a wide range of wall thicknesses. Chen et al. (2017) used the incremental theory to investigate instabilities of functionally graded tubes under combined axial stretch and internal or external pressures. Their parametric study highlights how graded material properties and loading conditions affect bifurcation behavior, enabling the design of soft cylindrical structures with tailored mechanical responses. Liu (2018) explored buckling of hyperelastic tubes under constrained compression and identified transition between axial and circumferential instabilities.

In addition to stress generated by external loads, a residual stress may develop in biological tissue due to growth and remodeling and in synthetic materials due to discontinuities between different components and the fabrication process. These additional stresses are in equilibrium with zero surface traction and persist even after external loads are removed. A well-known example is arterial tissue, which exhibits axial, circumferential, and radial residual stress components (Vaishnav and Vossoughi, 1987; Holzapfel and Ogden, 2010). It turns out that residual stress in arteries serves to homogenize stress distributions induced by blood pressure (Liu and Fung, 1989; Fung, 1991, 1993). Studies including the effect of residual stress in cardiac tissue have been carried in Omens and Fung (1990); Costa et al. (1997); Rausch and Kuhl (2013).

It is well known that the mechanical properties of residually stressed biological tissue are deformation dependent. To capture this behavior, Hoger (1985, 1993, 1996, 1997) developed a nonlinear elasticity theory to account for finite deformation and residual stress. Using Hoger’s work as starting point, Merodio et al. (2013) analyzed the influence of residual stress on the finite deformation of hyperelastic materials, focusing on problems such as simple shear, tube inflation, and tension-torsion of cylinders. Ahamed et al. (2016) investigated how residual stress affects wall stress distribution in abdominal aortic aneurysms (AAAs), using patient-specific data and

modeling the material as fiber-reinforced. Dorfmann and Ogden (2021) studied the impact of residual stress on the stability of pressurized tubes under axial extension, focusing on axisymmetric modes. Melnikov et al. (2021) conducted a detailed bifurcation analysis of residually stressed tubes subjected to combined extension and inflation, considering both axisymmetric and asymmetric responses. More recently, Liu and Dorfmann (2024) demonstrated that residual stress can trigger localized instabilities in a stretched cylinder and derived an analytical bifurcation condition for localization. Furthermore, both localized bulging and necking may occur, depending on the loading strategy (Liu and Dorfmann, 2024; Liu et al., 2024).

The focus of this work is provide a comprehensive investigation of the bifurcation behavior of tubes under axial compression, with particular attention to both axial and circumferential instability modes. We specialize the incremental equations and boundary conditions in Stroh form to derive an exact bifurcation condition and to investigate how residual stress influences the onset of buckling. The rest of this paper is organized as follows. Section 2 summarizes the fundamental theory for residually stressed solids. Section 3 outlines the incremental theory used for the bifurcation analysis. In Section 4, we examine compression of a residually stressed cylindrical tube, characterize the primary deformation, and derive the bifurcation condition using the Stroh formalism and surface impedance matrix method. A comprehensive parametric analysis of various buckling modes is presented in Section 5. Concluding remarks are given in Section 6.

2. Fundamental theory

The objective of this work is to investigate buckling instability of a compressed hyperelastic tube in the presence of residual stress. It is shown by Rajagopal and Wineman (2024); Bustamante et al. (2024) that residual stress or prestress in an elastic body can significantly alter its effective material symmetry, leading to an anisotropic mechanical response, even when the material is initially isotropic.

We consider a residually stressed body which, without external mechanical loads, occupies the reference configuration \mathcal{B}_r . When subjected to mechanical loads, the body undergoes finite deformation to occupy the current configuration, denoted \mathcal{B}_e . We introduce the position vectors \mathbf{X} and \mathbf{x} to identify a material point in the reference and current configurations, respectively. The deformation from \mathcal{B}_r to \mathcal{B}_e is written as $\mathbf{x} = \boldsymbol{\chi}(\mathbf{X})$. The deformation gradient \mathbf{F} is given by $\mathbf{F} = \text{Grad } \boldsymbol{\chi}$, where Grad is the gradient operator with respect to \mathbf{X} . The associated right and left Cauchy-Green deformation tensors, denoted \mathbf{C} and \mathbf{B} , respectively, are defined by

$$\mathbf{C} = \mathbf{F}^T \mathbf{F} \quad \mathbf{B} = \mathbf{F} \mathbf{F}^T, \quad (2.1)$$

where the superscript T indicates the transpose of a second-order tensor. For an incompressible material, we have

$$J = \det \mathbf{F} = 1. \quad (2.2)$$

2.1. Equilibrium and residual stress

We assume that there are no body forces and no intrinsic couple stresses. Then, the Cauchy stress $\boldsymbol{\sigma}$ is symmetric and satisfies the equilibrium equation

$$\text{div } \boldsymbol{\sigma} = \mathbf{0}, \quad (2.3)$$

where div is the divergence operator with respect to $\mathbf{x} \in \mathcal{B}_e$. The mechanical traction on the current boundary $\partial \mathcal{B}_e$ is specified by

$$\boldsymbol{\sigma} \mathbf{n} = \mathbf{t}_a \quad \text{on } \partial \mathcal{B}_e, \quad (2.4)$$

where \mathbf{n} denotes the outward unit normal vector.

To obtain the equivalent Lagrangian form, we first recall Nanson's formula (Ogden, 1997)

$$\mathbf{n}ds = J\mathbf{F}^{-T}\mathbf{N}dS, \quad (2.5)$$

which connects an infinitesimal area element ds with outward unit normal vector \mathbf{n} in the current configuration to the corresponding area element dS with outward unit normal vector \mathbf{N} in the reference configuration. Using equations (2.4) and (2.5), we find that

$$\mathbf{t}_a ds = \boldsymbol{\sigma} \mathbf{n} ds = J\mathbf{F}^{-1}\boldsymbol{\sigma}\mathbf{N}dS = \mathbf{T}^T\mathbf{N}dS, \quad (2.6)$$

where \mathbf{T} denotes the nominal stress

$$\mathbf{T} = J\mathbf{F}^{-1}\boldsymbol{\sigma}. \quad (2.7)$$

It satisfies the equilibrium equation

$$\text{Div}\mathbf{T} = \mathbf{0}, \quad (2.8)$$

where Div denotes the divergence operator defined in the reference configuration \mathcal{B}_r . The Lagrangian form of the traction boundary condition reads

$$\mathbf{T}^T\mathbf{N} = \mathbf{t}_A, \quad \text{on } \partial\mathcal{B}_r, \quad (2.9)$$

where \mathbf{t}_A is the load per unit surface area on \mathcal{B}_r and \mathbf{N} is the outward unit normal vector.

Let the reference configuration \mathcal{B}_r have a residual stress $\boldsymbol{\tau}$. Then, there is no distinction between different measures and we have $\mathbf{T} = \boldsymbol{\sigma} = \boldsymbol{\tau}$. From (2.8) we obtain

$$\text{Div}\boldsymbol{\tau} = \mathbf{0}, \quad (2.10)$$

with zero traction forces. Hence (2.9) gives

$$\boldsymbol{\tau}\mathbf{N} = \mathbf{0}, \quad \text{on } \partial\mathcal{B}_r, \quad (2.11)$$

with $\boldsymbol{\tau} = \boldsymbol{\tau}^T$.

2.2. Constitutive equations

For a residually stressed elastic solid, the strain energy density per unit volume is a function of the deformation gradient \mathbf{F} and the residual stress $\boldsymbol{\tau}$, which is written as $W(\mathbf{F}, \boldsymbol{\tau})$. Note that W is objective since it depends on \mathbf{F} only via the right Cauchy-Green deformation tensor \mathbf{C} and $\boldsymbol{\tau}$ is unaffected by rotations in the deformed configuration \mathcal{B}_e . The Cauchy and the nominal stresses are given by

$$\boldsymbol{\sigma} = \mathbf{F} \frac{\partial W}{\partial \mathbf{F}}(\mathbf{F}, \boldsymbol{\tau}) - p\mathbf{I}, \quad \mathbf{T} = \frac{\partial W}{\partial \mathbf{F}}(\mathbf{F}, \boldsymbol{\tau}) - p\mathbf{F}^{-1}, \quad (2.12)$$

respectively, where p is the Lagrange multiplier associated with the incompressibility constraint (2.2). In \mathcal{B}_r , when $\mathbf{F} = \mathbf{I}$, equation (2.12) reduces to

$$\boldsymbol{\tau} = \frac{\partial W}{\partial \mathbf{F}}(\mathbf{I}, \boldsymbol{\tau}) - p_r\mathbf{I}, \quad (2.13)$$

where p_r is the Lagrange multiplier in \mathcal{B}_r .

According to the continuum theory of anisotropic materials given by Spencer (1971) and generalized to residually stressed materials (Hoger, 1996, 1997), the strain energy function $W(\mathbf{C}, \boldsymbol{\tau})$ depends on 9 independent invariants of \mathbf{C} , $\boldsymbol{\tau}$ and their combinations. The principal invariants of \mathbf{C} are given by

$$I_1 = \text{tr } \mathbf{C}, \quad I_2 = \frac{1}{2} [I_1^2 - \text{tr } (\mathbf{C}^2)], \quad I_3 = \det \mathbf{C}, \quad (2.14)$$

and $I_3 = 1$ according to the incompressibility condition (2.2). The invariants for $\boldsymbol{\tau}$ independent of the deformation are collectively denoted by

$$I_4 = \{\text{tr } \boldsymbol{\tau}, \frac{1}{2} [(\text{tr } \boldsymbol{\tau})^2 - \text{tr } (\boldsymbol{\tau}^2)]\}, \quad \det \boldsymbol{\tau}\}. \quad (2.15)$$

There exist four additional invariants that depend on \mathbf{C} and $\boldsymbol{\tau}$ defined by

$$I_5 = \text{tr } (\boldsymbol{\tau} \mathbf{C}), \quad I_6 = \text{tr } (\boldsymbol{\tau} \mathbf{C}^2), \quad I_7 = \text{tr } (\boldsymbol{\tau}^2 \mathbf{C}), \quad I_8 = \text{tr } (\boldsymbol{\tau}^2 \mathbf{C}^2). \quad (2.16)$$

To indicate the dependence of W on the invariants (2.14)-(2.16) we write

$$W = W(I_1, I_2, I_4, I_5, I_6, I_7, I_8), \quad (2.17)$$

where $I_3 = 1$ and is therefore excluded. The nominal and Cauchy stresses are the obtained by

$$\mathbf{T} = \sum_{i \in \mathcal{I}} W_i \frac{\partial I_i}{\partial \mathbf{F}} - p \mathbf{F}^{-1}, \quad \boldsymbol{\sigma} = \mathbf{F} \mathbf{T}, \quad (2.18)$$

where $W_i = \partial W / \partial I_i$ and $\mathcal{I} = \{1, 2, 5, 6, 7, 8\}$. Expanding gives the explicit expression of the Cauchy stress tensor

$$\begin{aligned} \boldsymbol{\sigma} = & 2W_1 \mathbf{B} + 2W_2 (I_1 \mathbf{B} - \mathbf{B}^2) + 2W_5 \boldsymbol{\Sigma} + 2W_6 (\boldsymbol{\Sigma} \mathbf{B} + \mathbf{B} \boldsymbol{\Sigma}) \\ & + 2W_7 \boldsymbol{\Xi} + 2W_8 (\boldsymbol{\Xi} \mathbf{B} + \mathbf{B} \boldsymbol{\Xi}) - p \mathbf{I}. \end{aligned} \quad (2.19)$$

where we introduced the short-hand notations $\boldsymbol{\Sigma} = \mathbf{F} \boldsymbol{\tau} \mathbf{F}^T$ and $\boldsymbol{\Xi} = \mathbf{F} \boldsymbol{\tau}^2 \mathbf{F}^T$.

In the reference configuration \mathcal{B}_r , the invariants in (2.14) and (2.16) assume the values

$$I_1 = I_2 = 3, \quad I_5 = I_6 = \text{tr } \boldsymbol{\tau}, \quad I_7 = I_8 = \text{tr } (\boldsymbol{\tau}^2), \quad (2.20)$$

and (2.19) reduces to

$$\boldsymbol{\tau} = (2W_1 + 4W_2 - p_r) \mathbf{I} + 2(W_5 + 2W_6) \boldsymbol{\tau} + 2(W_7 + 2W_8) \boldsymbol{\tau}^2. \quad (2.21)$$

This requires that the energy function in \mathcal{B}_r is restricted to

$$2W_1 + 4W_2 - p_r = 0, \quad W_5 + 2W_6 = \frac{1}{2}, \quad W_7 + 2W_8 = 0, \quad (2.22)$$

see, for example, Shams et al. (2011); Dorfmann and Ogden (2021) for details.

3. Incremental theory

Here we provide a brief summery of the incremental theory and refer to, for example, Ogden (1997) for details. The buckling analysis is then reduced to studying the linearized increment in the deformation superimposed on a finitely deformed configuration subjected to a residual stress.

Consider an increment in the displacement, denoted $\dot{\mathbf{x}} = \dot{\boldsymbol{\chi}}(\mathbf{X})$, superimposed on the current configuration \mathcal{B}_e and resulting in an increment in the deformation gradient $\dot{\mathbf{F}} = \text{Grad} \dot{\boldsymbol{\chi}}$. We use a superposed dot to indicate an incremental quantity, see, for example, Haughton and Ogden (1979b), Hoger (1997), Melnikov et al. (2021), Dorfmann and Ogden (2021), Liu and Dorfmann (2024).

For what follows, it is convenient to write the increment of the displacement $\dot{\mathbf{x}}$ in Eulerian form resulting in an increment as a function of \mathbf{x} . This is obtained via the transformation

$$\mathbf{u}(\mathbf{x}) = \mathbf{u}(\boldsymbol{\chi}(\mathbf{X})) = \dot{\mathbf{x}}(\mathbf{X}). \quad (3.1)$$

The increment of equation (2.2) gives $\dot{J} = J \text{tr}(\mathbf{F}^{-1} \dot{\mathbf{F}}) = 0$, and we obtain the incremental form of the incompressibility condition

$$\text{tr} \mathbf{L} \equiv \text{div} \mathbf{u} = 0, \quad (3.2)$$

with

$$\mathbf{L} = \dot{\mathbf{F}} \mathbf{F}^{-1} = \text{grad} \mathbf{u} \quad (3.3)$$

being the incremental displacement gradient, and grad the gradient operator with respect to \mathcal{B}_e .

The incremental deformation generates an increment in the nominal stress, denoted by $\dot{\mathbf{T}}$, which satisfies the equation of equilibrium

$$\text{Div} \dot{\mathbf{T}} = \mathbf{0}, \quad (3.4)$$

and the associated incremental form of the boundary condition

$$\dot{\mathbf{T}}^T \mathbf{N} = \dot{\mathbf{t}}_A, \quad \text{on } \partial \mathcal{B}_r. \quad (3.5)$$

To write the incremental forms of the equilibrium equation and boundary conditions as a function of \mathbf{x} , we use the push-forward operation applied to $\dot{\mathbf{T}}$ and obtain $\dot{\mathbf{T}}_0 = \mathbf{F} \dot{\mathbf{T}}$. Accordingly, (3.4) transforms to

$$\text{div} \dot{\mathbf{T}}_0 = \mathbf{0}, \quad (3.6)$$

and (3.5) becomes

$$\dot{\mathbf{T}}_0^T \mathbf{n} = \dot{\mathbf{t}}_{a0}, \quad \text{on } \partial \mathcal{B}_e, \quad (3.7)$$

where $\dot{\mathbf{t}}_{a0}$ represents the increment of the mechanical traction in the current configuration.

Let $\{\mathbf{e}_1, \mathbf{e}_2, \mathbf{e}_3\}$ be an orthonormal basis for an orthogonal curvilinear coordinate system. Then, in component form, equation (3.6) yields the three scalar equations:

$$\dot{T}_{0ji,j} + \dot{T}_{0ji} \mathbf{e}_k \cdot \mathbf{e}_{j,k} + \dot{T}_{0kj} \mathbf{e}_i \cdot \mathbf{e}_{j,k} = 0, \quad i = 1, 2, 3, \quad (3.8)$$

where subscripts following a comma indicate partial derivatives and where the standard summation convention over repeated indices applies.

An increment in the deformation $\dot{\mathbf{x}}$ results in an incremental in the nominal stress. For an incompressible material this is given by

$$\dot{\mathbf{T}} = \mathcal{A}\dot{\mathbf{F}} + p\mathbf{F}^{-1}\dot{\mathbf{F}}\mathbf{F}^{-1} - \dot{p}\mathbf{F}^{-1}, \quad (3.9)$$

where \dot{p} is the increment of the Lagrange multiplier and \mathcal{A} is the fourth-order elastic moduli tensor with components

$$\mathcal{A}_{\alpha i \beta j} = \frac{\partial^2 W}{\partial F_{i\alpha} \partial F_{j\beta}}, \quad (3.10)$$

with the symmetry $\mathcal{A}_{\alpha i \beta j} = \mathcal{A}_{\beta j \alpha i}$. The updated version of (3.9) reads

$$\dot{\mathbf{T}}_0 = \mathcal{A}_0 \mathbf{L} + p\mathbf{L} - \dot{p}\mathbf{I}, \quad (3.11)$$

where the components of the updated elastic moduli tensor \mathcal{A}_0 are calculated as

$$\mathcal{A}_{0lkji} = \mathcal{A}_{0jilk} = F_{j\alpha} F_{l\beta} \mathcal{A}_{\alpha i \beta k}. \quad (3.12)$$

In terms of invariants the updated elasticity tensor has the expanded component form

$$\mathcal{A}_{0piqj} = \sum_{r \in \mathcal{I}} W_r F_{p\alpha} F_{q\beta} \frac{\partial^2 I_r}{\partial F_{i\alpha} \partial F_{j\beta}} + \sum_{r,s \in \mathcal{I}} W_{rs} F_{p\alpha} F_{q\beta} \frac{\partial I_r}{\partial F_{i\alpha}} \frac{\partial I_s}{\partial F_{j\beta}}, \quad (3.13)$$

where $W_{ij} = \partial W / \partial I_i \partial I_j$ with $i, j \in \mathcal{I}$. The expansion of \mathcal{A}_{0piqj} is given in Melnikov et al. (2021). We note that the components \mathcal{A}_{0piqj} are functions of residual stress (Destrade and Ogden, 2013).

4. Illustration

To obtain explicit results, we consider a residually stressed neo-Hookean material with the mechanical properties specified by the energy function

$$W = \frac{1}{2}\mu(I_1 - 3) + \frac{1}{2}(I_5 - \text{tr } \boldsymbol{\tau}) + \frac{1}{4}\xi(I_5 - \text{tr } \boldsymbol{\tau})^2, \quad (4.1)$$

where $\mu > 0$ is the shear modulus in the reference configuration and ξ is a non-negative material constant. It is easy to see that (4.1) satisfies the restriction in (2.22). Note that this model has been used by Dorfmann and Ogden (2021) to report on the restrictions imposed by the strong ellipticity condition and by Liu and Dorfmann (2024) to analyze localized instabilities of a residually stressed solid cylinder.

4.1. Primary deformation

Consider a homogeneous, hyperelastic and incompressible thick-walled tube whose reference configuration \mathcal{B}_r is given in terms of cylindrical polar coordinates (R, Θ, Z) by

$$A \leq R \leq B, \quad 0 \leq \Theta \leq 2\pi, \quad 0 \leq Z \leq L, \quad (4.2)$$

where A, B are the inner and outer radii and L is the reference length. The application of external loads results in the deformed configuration specified by

$$a \leq r \leq b, \quad 0 \leq \theta \leq 2\pi, \quad 0 \leq z \leq l, \quad (4.3)$$

where (r, θ, z) are the cylindrical polar coordinates, a, b the inner and outer deformed radii, $l = \lambda_z L$ is the current length and λ_z the axial stretch of the tube. The corresponding deformation gradient has the diagonal form

$$\mathbf{F} = \frac{dr}{dR} \mathbf{e}_r \otimes \mathbf{E}_r + \frac{r}{R} \mathbf{e}_\theta \otimes \mathbf{E}_\theta + \lambda_z \mathbf{e}_z \otimes \mathbf{E}_z, \quad (4.4)$$

where $\{\mathbf{E}_r, \mathbf{E}_\theta, \mathbf{E}_z\}$ and $\{\mathbf{e}_r, \mathbf{e}_\theta, \mathbf{e}_z\}$ are the orthonormal basis vectors in the reference and current configurations, respectively. Using $(2.1)_1$ gives the right Cauchy-Green deformation tensor

$$\mathbf{C} = \frac{R^2}{r^2 \lambda_z^2} \mathbf{E}_R \otimes \mathbf{E}_R + \frac{r^2}{R^2} \mathbf{E}_\Theta \otimes \mathbf{E}_\Theta + \lambda_z^2 \mathbf{E}_Z \otimes \mathbf{E}_Z, \quad (4.5)$$

where we used the incompressibility condition (2.2) in the form

$$r \lambda_z dr = R dR. \quad (4.6)$$

This, after integration gives

$$r^2 = \lambda_z^{-1} (R^2 - A^2) + a^2, \quad (4.7)$$

where a is to be determined.

Consider an axisymmetric residual stress distribution in \mathcal{B}_r with nonzero components τ_{RR} and $\tau_{\Theta\Theta}$. Then, (2.10) reduces to the non-zero component equation

$$\frac{d\tau_{RR}}{dR} + \frac{1}{R} (\tau_{RR} - \tau_{\Theta\Theta}) = 0, \quad (4.8)$$

and the zero traction boundary condition (2.11) specializes to

$$\tau_{RR} = 0, \quad \text{on } \partial\mathcal{B}_r \quad (4.9)$$

The invariants I_1, I_5 used in the energy function (4.1) have the forms

$$\begin{aligned} I_1 &= \frac{R^2}{r^2 \lambda_z^2} + \frac{r^2}{R^2} + \lambda_z^2, \\ I_5 &= \frac{R^2}{r^2 \lambda_z^2} \tau_{RR} + \frac{r^2}{R^2} \tau_{\Theta\Theta}, \end{aligned} \quad (4.10)$$

which are used to evaluate the components of the Cauchy stress (2.19)

$$\begin{aligned} \sigma_{rr} &= \mu \frac{R^2}{r^2 \lambda_z^2} + \left\{ 1 + \xi \left[\left(\frac{R^2}{r^2 \lambda_z^2} - 1 \right) \tau_{RR} + \left(\frac{r^2}{R^2} - 1 \right) \tau_{\Theta\Theta} \right] \right\} \frac{R^2}{r^2 \lambda_z^2} \tau_{RR} - p, \\ \sigma_{\theta\theta} &= \mu \frac{r^2}{R^2} + \left\{ 1 + \xi \left[\left(\frac{R^2}{r^2 \lambda_z^2} - 1 \right) \tau_{RR} + \left(\frac{r^2}{R^2} - 1 \right) \tau_{\Theta\Theta} \right] \right\} \frac{r^2}{R^2} \tau_{\Theta\Theta} - p, \\ \sigma_{zz} &= \mu \lambda_z^2 - p. \end{aligned} \quad (4.11)$$

These must satisfy equilibrium (2.3), which reduces to the component equation

$$\frac{d\sigma_{rr}}{dr} + \frac{\sigma_{rr} - \sigma_{\theta\theta}}{r} = 0 \quad (4.12)$$

that can be integrated to obtain

$$\sigma_{rr} = \int_a^r \frac{\sigma_{\theta\theta} - \sigma_{rr}}{r} dr, \quad (4.13)$$

where the lower limit a is obtained from the traction-free condition on $r = a$. In view of the traction-free condition on $r = b$, we obtain

$$\int_a^b \frac{\sigma_{\theta\theta} - \sigma_{rr}}{r} dr = 0, \quad (4.14)$$

where (4.7) connects b and R to a . It follows from (4.11)₁ and (4.13) that the Lagrange multiplier p is obtained by

$$p = \mu \frac{R^2}{r^2 \lambda_z^2} + \left\{ 1 + \xi \left[\left(\frac{R^2}{r^2 \lambda_z^2} - 1 \right) \tau_{RR} + \left(\frac{r^2}{R^2} - 1 \right) \tau_{\Theta\Theta} \right] \right\} \frac{R^2}{r^2 \lambda_z^2} \tau_{RR} - \int_a^r \frac{\sigma_{\theta\theta} - \sigma_{rr}}{r} dr. \quad (4.15)$$

To evaluate (4.13), explicit expressions of the residual stress components τ_{RR} , $\tau_{\Theta\Theta}$ that satisfy equilibrium (4.8) and the boundary condition (4.9) are needed. For the radial component we use

$$\tau_{RR} = \zeta (R - A) (R - B), \quad (4.16)$$

where ζ is a constant that defines the magnitude of the residual stress, see, for example, Dorfmann and Ogden (2021); Merodio and Ogden (2016). We note that $\tau_{RR} < 0$ for $\zeta > 0$. For the circumferential component $\tau_{\Theta\Theta}$ we use (4.8) resulting in

$$\tau_{\Theta\Theta} = \zeta [3R^2 - 2(A + B)R + AB]. \quad (4.17)$$

It is convenient to take λ_z as the loading parameter and use (4.14) to obtain an implicit function connecting a to λ_z , denoted $f(a, \lambda_z, \zeta) = 0$. Once a is identified, the deformed outer radius is given by (4.7) and the primary deformation is fully characterized.

To explore the influence of the residual stress on the primary deformation we first consider the case where $\zeta = 0$. The constitutive equation (4.1) then specializes to the neo-Hookean model and the compression-induced primary deformation becomes homogeneous (Wilkes, 1955; Dai and Wang, 2008; Dai et al., 2015).

To investigate the effect of residual stress we introduce the dimensionless parameters κ, ν defined by

$$\kappa = \xi \mu, \quad \nu = \frac{\zeta A^2}{\mu}, \quad (4.18)$$

which are used in the subsequent analysis. In Figure 1 we show the normalized inner and outer radii a/A and b/A as a function of the axial stretch λ_z for the values $\kappa = 0.5$ and $\nu = 10$. Note that the dashed curves monotonically increase with the compression stretch λ_z , indicating that the outer surface continuously expands. The inner radius, for $B/A = 1.01$ and 1.2 , shows a similar behavior. However, for larger values of B/A a non-monotonic behavior is observed. Therefore, the inner surface first moves towards the center and then reverses direction for increasing compression. For a constant value of B/A , the transition point depends on the residual stress and can be obtained when the derivative of $a(\lambda_z)$ with respect to λ_z vanishes at $\lambda_z = 1$. With reference to the implicit function $f(a, \lambda_z, \zeta) = 0$ we use

$$\left. \frac{\partial f(a, \lambda_z, \nu_{tr})}{\partial \lambda_z} \right|_{\lambda_z=1, a=A} = 0, \quad (4.19)$$

to obtain the transition value ν_{tr} . Representative values are listed in Table 1 and illustrated as a function of B/A in the right panel in Figure 1. Hence, the residual stress plays a significant role in the primary deformation with its impact becoming more pronounced for increasing wall thickness.

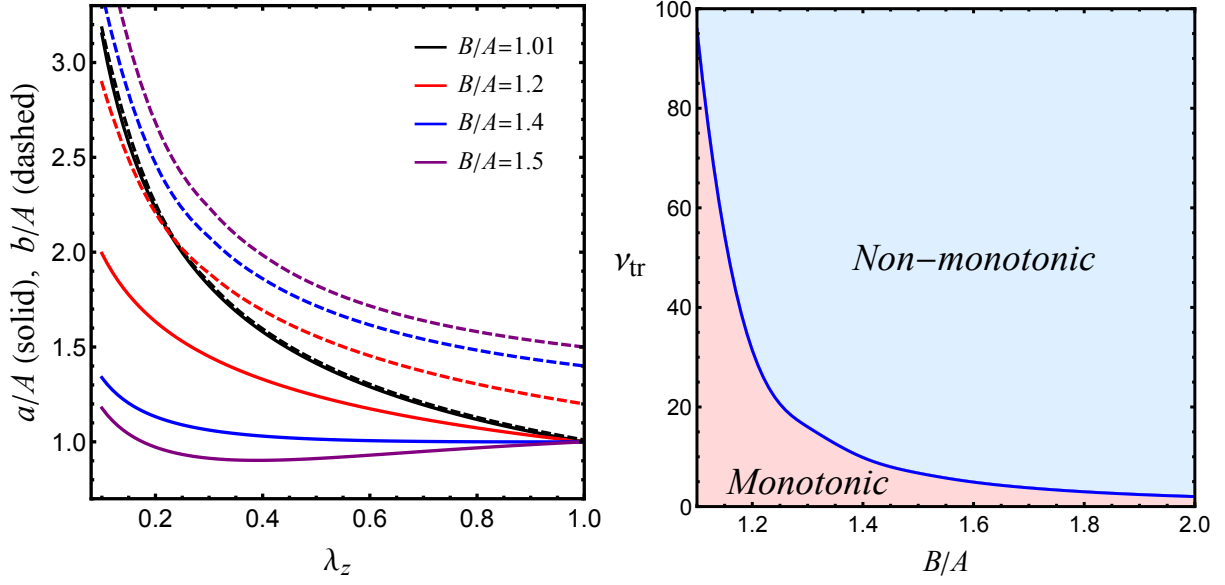


Figure 1: The left panel shows the dependence of the normalized inner and outer radii on λ_z for $\nu = 10$ and $\kappa = 0.5$. The one on the right the transition value ν_{tr} as a function of B/A for $\kappa = 0.5$.

Table 1: The transition residual stress parameter ν_{tr} for different values of B/A .

B/A	1.1	1.2	1.3	1.4	1.5	1.6	1.7	1.8	1.9	2.0
ν_{tr}	95.3710	31.2297	15.9761	9.8409	6.7217	4.9057	3.7501	2.9666	2.4096	1.9989

4.2. Bifurcation analysis

We now specialize the incremental theory summarized in Section 3 to perform a buckling analysis of an axially compressed tube. We take the incremental displacement vector \mathbf{u} as

$$\mathbf{u} = u \mathbf{e}_r + v \mathbf{e}_\theta + w \mathbf{e}_z, \quad (4.20)$$

which gives the incremental displacement gradient (3.3) in matrix form

$$\mathbf{L} = \begin{bmatrix} \frac{\partial u}{\partial r} & \frac{1}{r} \frac{\partial u}{\partial \theta} - \frac{v}{r} & \frac{\partial u}{\partial z} \\ \frac{\partial v}{\partial r} & \frac{1}{r} \frac{\partial v}{\partial \theta} + \frac{u}{r} & \frac{\partial v}{\partial z} \\ \frac{\partial w}{\partial r} & \frac{1}{r} \frac{\partial w}{\partial \theta} & \frac{\partial w}{\partial z} \end{bmatrix}, \quad (4.21)$$

and the linearized incremental incompressibility condition (3.2)

$$\text{tr } \mathbf{L} = \frac{\partial u}{\partial r} + \frac{1}{r} \frac{\partial v}{\partial \theta} + \frac{u}{r} + \frac{\partial w}{\partial z} = 0. \quad (4.22)$$

The components of the incremental equation (3.8) become

$$\begin{aligned}\dot{T}_{011,1} + \dot{T}_{021,2} + \dot{T}_{031,3} + (\dot{T}_{011} - \dot{T}_{022})/r &= 0, \\ \dot{T}_{012,1} + \dot{T}_{022,2} + \dot{T}_{032,3} + (\dot{T}_{012} + \dot{T}_{021})/r &= 0, \\ \dot{T}_{013,1} + \dot{T}_{023,2} + \dot{T}_{033,3} + \dot{T}_{013}/r &= 0,\end{aligned}\tag{4.23}$$

where we renamed the coordinate directions r, θ, z as 1, 2, 3, respectively. From (3.7) the traction-free boundary condition specializes to

$$\dot{T}_{011} = 0, \quad \dot{T}_{012} = 0, \quad \dot{T}_{013} = 0, \quad \text{on } r = a, b.\tag{4.24}$$

Following Wilkes (1955) and Chen et al. (2017), we assume that the two ends remain planar during deformation and impose sliding boundary conditions resulting in

$$\frac{\partial w}{\partial \theta} = 0, \quad \frac{\partial w}{\partial r} = 0, \quad \dot{T}_{031} = 0, \quad \dot{T}_{032} = 0, \quad \text{on } z = 0, l.\tag{4.25}$$

The Eulerian form of the incremental stress components in (3.11) have the explicit forms

$$\begin{aligned}\dot{T}_{011} &= (\mathcal{A}_{01111} + p)L_{11} + \mathcal{A}_{01122}L_{22} + \mathcal{A}_{01133}L_{33} - \dot{p}, \\ \dot{T}_{022} &= \mathcal{A}_{02211}L_{11} + (\mathcal{A}_{02222} + p)L_{22} + \mathcal{A}_{02233}L_{33} - \dot{p}, \\ \dot{T}_{033} &= \mathcal{A}_{03311}L_{11} + \mathcal{A}_{03322}L_{22} + (\mathcal{A}_{03333} + p)L_{33} - \dot{p}, \\ \dot{T}_{012} &= \mathcal{A}_{01212}L_{21} + (\mathcal{A}_{01221} + p)L_{12}, \\ \dot{T}_{021} &= \mathcal{A}_{02121}L_{12} + (\mathcal{A}_{02112} + p)L_{21}, \\ \dot{T}_{013} &= \mathcal{A}_{01313}L_{31} + (\mathcal{A}_{01331} + p)L_{13}, \\ \dot{T}_{031} &= \mathcal{A}_{03131}L_{13} + (\mathcal{A}_{03113} + p)L_{31}, \\ \dot{T}_{023} &= \mathcal{A}_{02323}L_{32} + (\mathcal{A}_{02332} + p)L_{23}, \\ \dot{T}_{032} &= \mathcal{A}_{03232}L_{23} + (\mathcal{A}_{03223} + p)L_{32}.\end{aligned}\tag{4.26}$$

In addition to the dimensionless parameters (4.18), we introduce the normalized quantities

$$\begin{aligned}\hat{r} &= \frac{r}{A}, \quad \hat{z} = \frac{z}{A}, \quad \hat{u} = \frac{u}{A}, \quad \hat{w} = \frac{w}{A}, \quad \hat{a} = \frac{a}{A}, \quad \hat{b} = \frac{b}{A}, \\ \hat{l} &= \frac{l}{A}, \quad \gamma = \frac{B}{L}, \quad \hat{T}_{0ij} = \frac{\dot{T}_{0ij}}{\mu}, \quad \hat{p} = \frac{p}{\mu}, \quad \hat{\dot{p}} = \frac{\dot{p}}{\mu}, \quad \hat{\mathcal{A}}_{0jilk} = \frac{\mathcal{A}_{0jilk}}{\mu}.\end{aligned}\tag{4.27}$$

For clarity, the hats on these variables will be dropped in the subsequent analysis.

To derive the bifurcation condition, we employ Stroh's method (Stroh, 1962) and look for periodic solutions of the form

$$\begin{aligned}u &= U(r) \cos m\theta \cos \alpha z, \quad v = V(r) \sin m\theta \cos \alpha z, \quad w = W(r) \cos m\theta \sin \alpha z, \\ r\dot{T}_{011} &= S_{11}(r) \cos m\theta \cos \alpha z, \quad r\dot{T}_{012} = S_{12}(r) \sin m\theta \cos \alpha z, \quad r\dot{T}_{013} = S_{13}(r) \cos m\theta \sin \alpha z,\end{aligned}\tag{4.28}$$

where m is the circumferential and α the axial wave number. The end conditions (4.25) result in

$$\alpha = \frac{n\pi}{l} = \frac{n\pi}{\lambda_z L/A} = \frac{\gamma n\pi}{\lambda_z B/A}, \quad n = 1, 2, 3, \dots,\tag{4.29}$$

where n denotes the normalized axial wave number. It will be shown that this selection connects γ and n and facilitates the bifurcation analysis by reducing the number of free parameters.

To write the equations in Stroh form, we define the displacement-traction vector $\boldsymbol{\eta}$ as

$$\boldsymbol{\eta}(r) = \begin{bmatrix} \mathbf{U}(r) \\ r\mathbf{S}(r) \end{bmatrix} \quad \text{where} \quad \begin{cases} \mathbf{U}(r) = [U(r), V(r), W(r)]^T, \\ \mathbf{S}(r) = [S_{11}(r), S_{12}(r), S_{13}(r)]^T. \end{cases} \quad (4.30)$$

We also take $\dot{p} = P(r) \cos m\theta \cos \alpha z$ and use of (4.28)₄ to obtain

$$P(r) = \frac{1}{r} (\mathcal{A}_{1122}(U(r) + mV(r)) - S_{11}(r) + r((\mathcal{A}_{1122} + p)U'(r) - \alpha\mathcal{A}_{1133}W(r))). \quad (4.31)$$

In addition, using (4.23)_{1,2} and (4.26)_{1,4,6}, we find that

$$\frac{d\boldsymbol{\eta}(r)}{dr} = \frac{1}{r}\mathbf{G}(r)\boldsymbol{\eta}(r), \quad (4.32)$$

which is known as the Stroh form of the governing equations. The Stroh matrix $\mathbf{G}(r)$ has the form

$$\mathbf{G}(r) = \begin{bmatrix} \mathbf{G}_1 & \mathbf{G}_2 \\ \mathbf{G}_3 & \mathbf{G}_4 \end{bmatrix}. \quad (4.33)$$

where $\mathbf{G}_i, i = \{1, 2, 3\}$ are 3×3 matrices, with \mathbf{G}_2 and \mathbf{G}_3 symmetric. In component form we have

$$\begin{aligned} \mathbf{G}_1 &= \begin{bmatrix} -1 & -m & -\alpha r \\ \frac{m(p + \mathcal{A}_{1221})}{\mathcal{A}_{1212}} & \frac{p + \mathcal{A}_{1221}}{\mathcal{A}_{1212}} & 0 \\ \frac{\alpha(p + \mathcal{A}_{1331})r}{\mathcal{A}_{1313}} & 0 & 0 \end{bmatrix}, \quad \mathbf{G}_2 = \begin{bmatrix} 0 & 0 & 0 \\ 0 & \frac{1}{\mathcal{A}_{1212}} & 0 \\ 0 & 0 & \frac{1}{\mathcal{A}_{1313}} \end{bmatrix}, \\ \mathbf{G}_3 &= \begin{bmatrix} g_{11} & g_{12} & g_{13} \\ g_{12} & g_{22} & g_{23} \\ g_{13} & g_{23} & g_{33} \end{bmatrix}, \quad \mathbf{G}_4 = -\mathbf{G}_1^T, \end{aligned} \quad (4.34)$$

where the components of \mathbf{G}_3 have the expressions

$$\begin{aligned} g_{11} &= \mathcal{A}_{1111} - 2\mathcal{A}_{1122} + \mathcal{A}_{2222} + \mathcal{A}_{2121}m^2 - \frac{m^2(\mathcal{A}_{1221} + p)^2}{\mathcal{A}_{1212}} - \frac{\alpha^2 r^2 (\mathcal{A}_{1331} + p)^2}{\mathcal{A}_{1313}} + 2p + \alpha^2 r^2 \mathcal{A}_{3131}, \\ g_{12} &= m \left(\mathcal{A}_{1111} - 2\mathcal{A}_{1122} + \mathcal{A}_{2121} + \mathcal{A}_{2222} - \frac{(\mathcal{A}_{1221} + p)^2}{\mathcal{A}_{1212}} + 2p \right), \\ g_{13} &= \alpha r (\mathcal{A}_{1111} - \mathcal{A}_{1133} - \mathcal{A}_{2211} + \mathcal{A}_{2233} + p), \\ g_{22} &= \mathcal{A}_{2121} + \mathcal{A}_{1111}m^2 - 2\mathcal{A}_{1122}m^2 + \mathcal{A}_{2222}m^2 + 2m^2p - \frac{(\mathcal{A}_{1221} + p)^2}{\mathcal{A}_{1212}} + \alpha^2 r^2 \mathcal{A}_{3232}, \\ g_{23} &= \alpha r (\mathcal{A}_{1111} - \mathcal{A}_{1133} - \mathcal{A}_{2211} + \mathcal{A}_{2233} + \mathcal{A}_{3232} + 2p)m, \\ g_{33} &= \mathcal{A}_{2323}m^2 + \alpha^2 r^2 (\mathcal{A}_{1111} - 2\mathcal{A}_{1133} + \mathcal{A}_{3333} + 2p). \end{aligned} \quad (4.35)$$

Without loss of generality, we assume that (4.32) admits six independent solutions $\boldsymbol{\eta}_i(r), i = \{1, \dots, 6\}$, which suggests to write a general solution as

$$\boldsymbol{\eta}(r) = \boldsymbol{\Gamma}(r)\mathbf{d}, \quad (4.36)$$

where

$$\mathbf{\Gamma}(r) = [\boldsymbol{\eta}_1, \boldsymbol{\eta}_2, \boldsymbol{\eta}_3, \boldsymbol{\eta}_4, \boldsymbol{\eta}_5, \boldsymbol{\eta}_6], \quad \mathbf{d} = [C_1, C_2, C_3, C_4, C_5, C_6]^T, \quad (4.37)$$

with C_i $\{i = 1, \dots, 6\}$ being arbitrary constants. For any $a \leq r_k \leq b$, we define

$$\mathbf{M}(r, r_k) = \mathbf{\Gamma}(r)\mathbf{\Gamma}^{-1}(r_k) = \begin{pmatrix} \mathbf{M}_1(r, r_k) & \mathbf{M}_2(r, r_k) \\ \mathbf{M}_3(r, r_k) & \mathbf{M}_4(r, r_k) \end{pmatrix}, \quad \mathbf{D} = \mathbf{\Gamma}(r_k)\mathbf{d}, \quad (4.38)$$

and rewrite the general solution as

$$\boldsymbol{\eta}(r) = \mathbf{M}(r, r_k)\mathbf{D}. \quad (4.39)$$

It is easy to show that $\mathbf{M}(r_k, r_k)$ is the 6×6 identity matrix. Then it follows from (4.32) that

$$\frac{d\mathbf{M}(r, r_k)}{dr} = \frac{1}{r}\mathbf{G}(r)\mathbf{M}(r, r_k). \quad (4.40)$$

We use the surface impedance matrix method and assume that there exists a conditional impedance matrix $\mathbf{z}(r)$ such that

$$r\mathbf{S}(r) = \mathbf{z}(r)\mathbf{u}(r). \quad (4.41)$$

For details we refer to, for example, (Shuvalov, 2003a,b; Norris and Shuvalov, 2010). On substituting (4.30) and (4.41) into (4.32) we obtain the Riccati equation

$$\frac{d}{dr}\mathbf{z} = \frac{1}{r}(\mathbf{G}_3 - \mathbf{G}_1^T\mathbf{z} - \mathbf{z}\mathbf{G}_1 - \mathbf{z}\mathbf{G}_2\mathbf{z}). \quad (4.42)$$

Taking $r_k = a$ and making use of the traction-free condition on $r = a$ gives

$$\mathbf{z} = \mathbf{M}_3\mathbf{M}_1^{-1}. \quad (4.43)$$

Since $\mathbf{M}_3(a) = 0$ we obtain $\mathbf{z}(a) = \mathbf{0}$, which yields the initial condition to numerically integrate (4.42) from $r = a$ to $r = b$. Traction-free boundary conditions on $r = b$ result in $\mathbf{z}(b)\mathbf{u}(b) = \mathbf{0}$ and in the bifurcation condition

$$\det[\mathbf{z}(b)] = 0, \quad (4.44)$$

which depends on the axial stretch λ_z , the residual stress parameter ν , the material parameter κ , the slenderness ratio $\gamma = B/L$, the mode numbers n, m , and the wall thickness ratio B/A . We use the software package *Mathematica* (Wolfram, Research, Inc., 2024) to solve the bifurcation condition (4.44) numerically.

5. Parametric study of the buckling behavior

In this section we consider tubes with slenderness ratio γ , with thickness ratio B/A and with residual stress and stiffness parameters ν and κ to evaluate the effect of the residual stress on the buckling behavior. When $\mathcal{A}_{1212} = 0$ or $\mathcal{A}_{1313} = 0$, special attention is necessary to treat the singularity when integrating (4.32) from $a < r < b$. With no residual stress $\mathcal{A}_{1212} = \mathcal{A}_{1313} = \lambda_z^{-1}$ and the singularity does not occur. However, as discussed in Liu and Dorfmann (2024), the residual stress generates at least one regular singular point. For a tube, this can be excluded by

limiting the wall thickness. We therefore restrict attention to a moderately thick-walled tube with $1 < B/A \leq 1.4$.

Note that the slenderness parameter γ and the axial wave number n appear together in the bifurcation condition, whose dependence on γ is through α , see (4.29). Therefore, it is convenient to treat γn as a single parameter setting $n = 1$. Then, in Figure 2 we illustrate the bifurcation curves for the dimensionless parameters $\kappa = 0.5$ and $B/A = 1.2$ and for different circumferential modes as a function of γ . The left and right panels illustrate the responses for $\nu = 5$ and $\nu = -5$, respectively. For fixed γ , the value of λ_z closed to unity gives the critical stretch. Following Springhetti et al. (2023), we depict the curves that provide the critical stretch as solid lines, known as intersecting modes. The results indicate that for increasing γ the critical wave number changes from $m = 1$ to $m = 2$ and then back to $m = 1$. For further increase in γ the barreling mode $m = 0$ occurs first. With no residual stress, the classical results of compressed tubes reported by, for example, Goriely et al. (2008); Springhetti et al. (2023) are recovered.

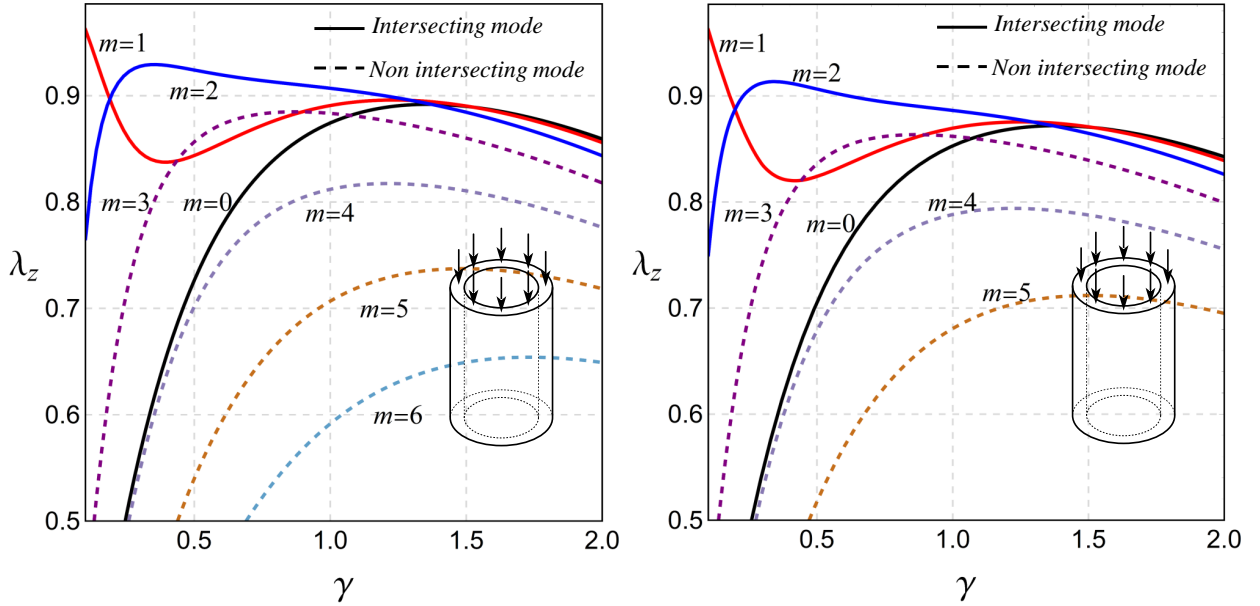


Figure 2: Bifurcation curves obtained from the condition (4.44) for various circumferential wave numbers. The panel on the left is for $\kappa = 0.5$, $B/A = 1.2$, $\nu = 5$. The results on the right are for $\kappa = 0.5$, $B/A = 1.2$, $\nu = -5$.

In Figure 3 we illustrate the bifurcation parameter λ_z as a function of γ for two values of B/A when $\kappa = 0.5$ and $\nu = 5$. The curves in the left panel are obtained for $B/A = 1.05$ and show that the critical mode changes from $m = 0$ to $m = 4$, depending on the slenderness ratio γ . The results on the right correspond to $B/A = 1.4$ and again show that the critical mode numbers depend on γ and are $m = 0, 1, 2$. Comparing to the results in Figure 2, we conclude that increasing wall-thickness delays the onset of instability. We also find the dependence of the critical stretch on the slenderness ratio γ complex due to mode transitions and, even for a fixed mode, the behavior of λ_z as a function of γ is non-monotonic. When $\gamma \rightarrow 0$, the tube approaches the membrane limit and Euler buckling $m = 1$ occurs in all cases. Conversely, as $\gamma \rightarrow \infty$, the critical stretch is attained when $m = 0$, similar to the results given in Wilkes (1955).

We now focus on the range of γ , where the barreling mode $m = 0$ occurs (Chau, 1995). In Figure 4 we illustrate the critical stretch λ_z as a function of γ for values of the dimensionless residual stress parameter $\nu = 0, 5, 10$. The dashed curves represent the regions where Euler buckling occurs and the dots indicate the transition to barreling. The curves in the left panel show that for a tube

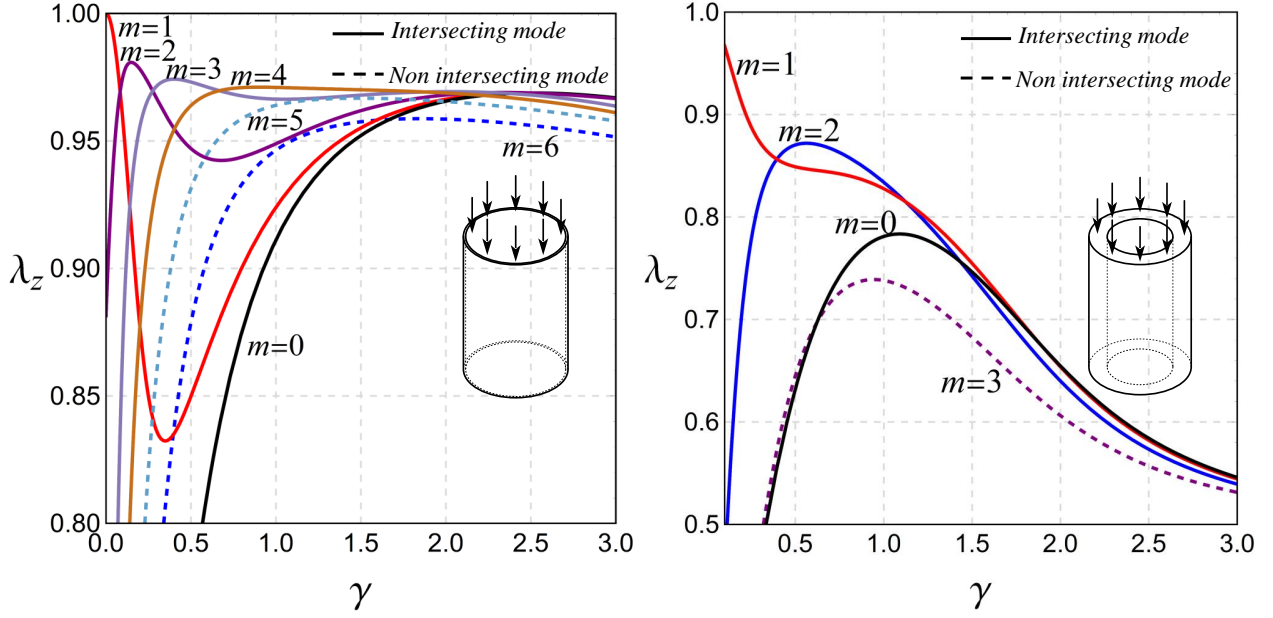


Figure 3: The critical stretch λ_z for different circumferential wave numbers. The results on the left are for $\kappa = 0.5$, $B/A = 1.05$, $\nu = 5$, the ones on the right for $\kappa = 0.5$, $B/A = 1.4$, $\nu = 5$.

with $B/A = 1.2$ the influence of the residual stress is essentially identical for all considered values of ν . The bifurcation curves on the right show that for a tube with $B/A = 1.4$ the residual stress leads to a delay in the emergence of the barreling mode, i.e., more compression is required. For $\nu = 10$, for example, the barreling mode is entirely suppressed, suggesting that a residual stress can effectively eliminate some instability modes.

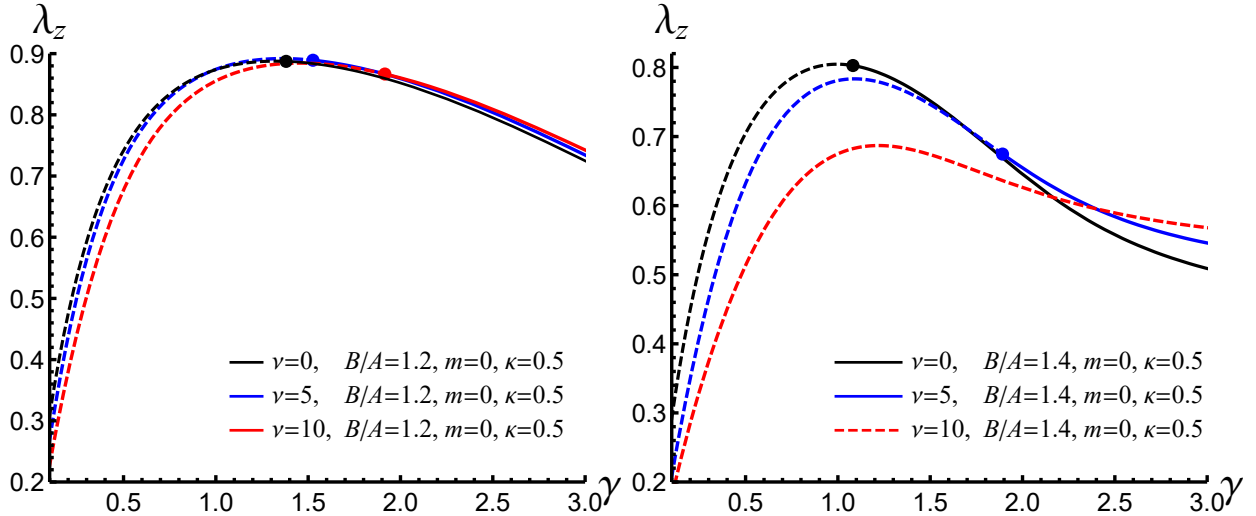


Figure 4: The critical stretch λ_z for barreling to occur as a function of the slenderness parameter γ for $\nu = 0, 5, 10$. The results shown in the left panel are for $\kappa = 0.5$ and $B/A = 1.2$, those on the right for $\kappa = 0.5$ and $B/A = 1.4$.

In Springhetti et al. (2023) it is shown that barreling instability can occur in the absence of residual stress. It is therefore of interest to determine the value of the dimensionless parameter ν necessary to suppress this mode of instability, see Figure 4. We take $\kappa = 0.5$, $B/A = 1.4$, select a

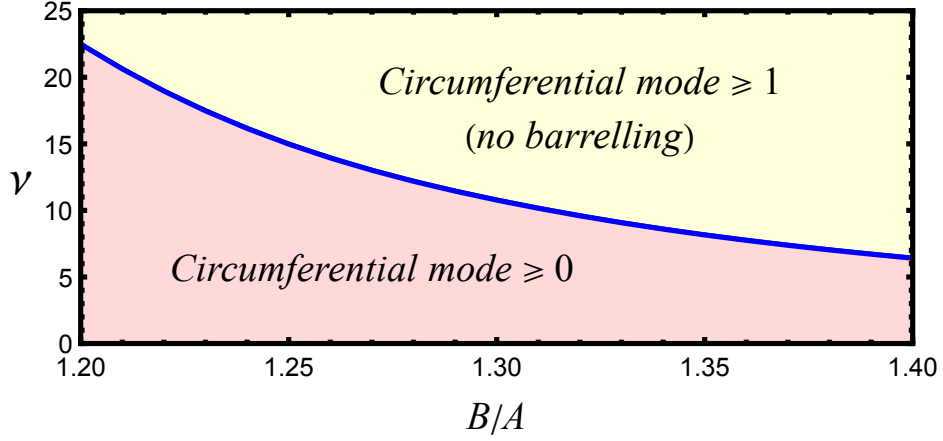


Figure 5: Phase diagram of different circumferential modes in the $\nu - B/A$ plane when $\kappa = 0.5$.

ratio γ and simultaneously solve the bifurcation condition for λ_z and ν

$$\det[\mathbf{z}(b)] \Big|_{m=0} = 0, \quad \det[\mathbf{z}(b)] \Big|_{m=1} = 0. \quad (5.1)$$

By varying γ we obtain a curve in the $\nu - \gamma$ plane representing the transition from the barreling mode $m = 0$ to the Euler buckling mode $m = 1$. This curve is non-monotonic and its maximum occurs at $\nu \approx 6.41$. Hence, for $\nu > 6.41$ the barreling mode is completely suppressed consistent with the results depicted in the right panel of Figure 4. Results obtained by varying the ratio B/A are shown in the phase diagram in Figure 5.

In Figure 6 we show the critical stretch λ_z as a function of the dimensionless parameter ν for the barreling mode $m = 0$, for $\kappa = 0.5$ and $\gamma = 2.5$. The results shown on the left are obtained when $B/A = 1.2$, the ones on the right when $B/A = 1.4$.

The horizontal line in each panel is used for reference and marks the critical stretch for a compressed tube with no residual stress. The results on the left are for $-15 \leq \nu \leq 22.49$ and show that negative values delay the onset of instability while positive values render the tube more unstable. For $\nu \approx 20.182$ the residual stress has no effect, with the critical stretch being identical to the tube with no residual stress. For $\nu > 20.182$ a delay in the onset of instability occurs.

The panel on the right shows the stability behavior for $-15 \leq \nu \leq 6.41$, where the upper limit represents the threshold beyond which the barreling mode no longer exists. The results show that the horizontal line and the curve intersect when $\nu \approx -10.398$ and $\nu \approx -1.353$, indicating that the residual stress has no effect on the tube stability. Bifurcation is delayed for $-15 \leq \nu \leq -10.398$ and $-1.353 \leq \nu \leq 0$. Outside these ranges the residual stress destabilizes the tube.

We now investigate the influence of the residual stress and slenderness ratio $\gamma = B/L$ on the Euler buckling mode $m = 1$ (Goriely et al., 2008; Zhou et al., 2023). From Figures 2 and 3 we find that this instability occurs for small values of γ , hence we focus on this region. Figure 7 shows the bifurcation curves for $m = 1$, $\kappa = 0.5$ and $\nu = 0, \pm 5, \pm 10$. The curves in the left panel are obtained when $B/A = 1.2$ and the ones on the right are for $B/A = 1.4$. The solid, black curves correspond to the bifurcation with no residual stress, which in all cases lie below the others. Therefore, the residual stress has a destabilizing effect. We also find that an increase in γ due to an increase in the outer radius or a reduction in the total length L stabilizes the tube. Comparing the left and right images we note that an increase in the wall-thickness amplifies the effect of the residual stress, which has negligible influence in very thin tubes.

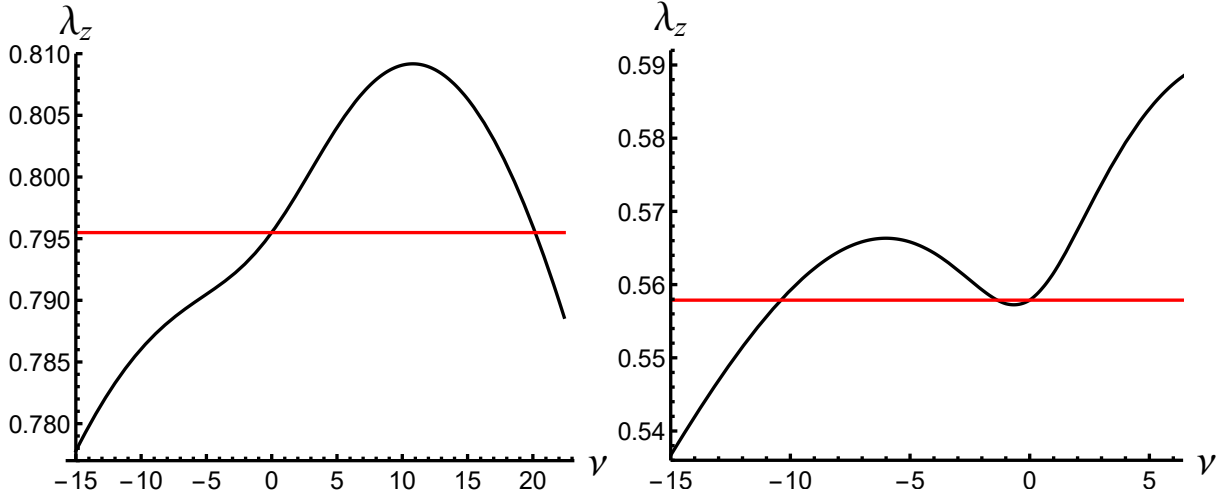


Figure 6: Dependence of the critical stretch of the barreling mode $m = 0$ on the residual stress ν , for $\kappa = 0.5$ and $\gamma = 2.5$. The results on the left are obtained when $B/A = 1.2$, the ones on the right when $B/A = 1.4$.

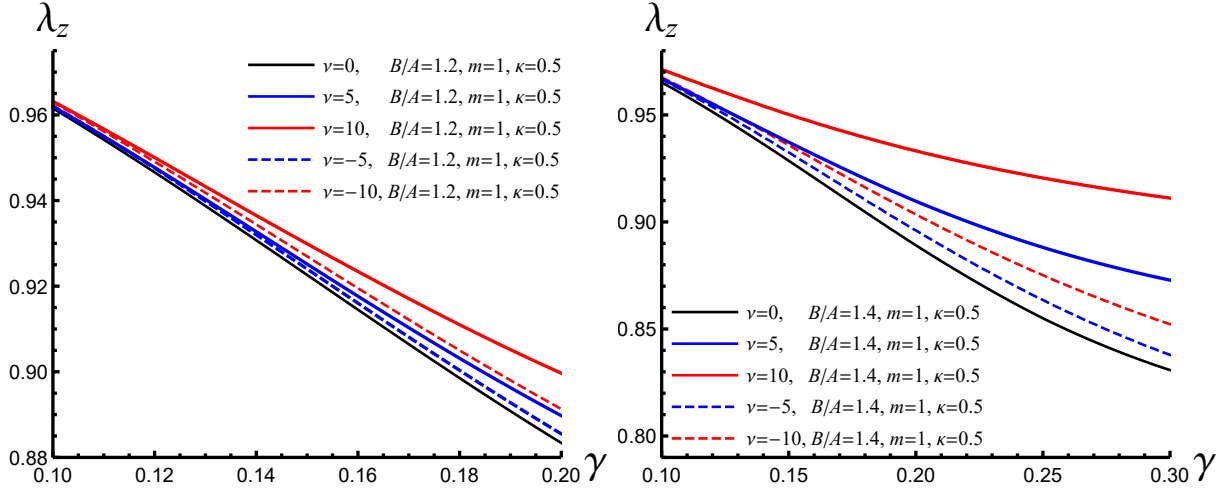


Figure 7: Bifurcation curves for the buckling mode $m = 1$ at different magnitudes of the residual stress ν . The parameters are set as (a) $\kappa = 0.5$, $B/A = 1.2$ and (b) $\kappa = 0.5$, $B/A = 1.4$.

In Figure 8 we depict the dependence of the critical stretch λ_z on the dimensionless residual stress parameter ν for the fixed value $\kappa = 0.5$. The curves from top to bottom correspond to slenderness ratios γ from 0.14 to 0.16 with increments of 0.005. Each curve has a minimum where $\nu \approx 0$ indicating that both positive and negative values of ν destabilize the tube.

In figures 2 and 3 we have shown that the buckling mode transitions from $m = 1$ to $m = 2$ as γ increases. Here we investigate how the residual stress effects mode $m = 2$ and illustrate the results in Figure 9. We plot the bifurcation curves for $m = 2$, $\kappa = 0.5$ and $\nu = 0, \pm 5, \pm 10$, on the left for $B/A = 1.2$ and on the right for $B/A = 1.4$. We note that the critical stretch λ_z exhibits a non-monotonic dependence on γ and that an increase in the wall-thickness amplifies the effect of the residual stress.

In Figure 10 we report the critical stretch λ_z for mode $m = 2$, $\kappa = 0.5$ as a function of the dimensionless residual stress parameter ν for $0.4 \leq \gamma \leq 0.6$ with increments of 0.05. We again depict the results for $B/A = 1.2$ in the left panel, for $B/A = 1.4$ on the right. The curves on the left show that the critical compression stretch decreases almost linearly with ν , on the right the

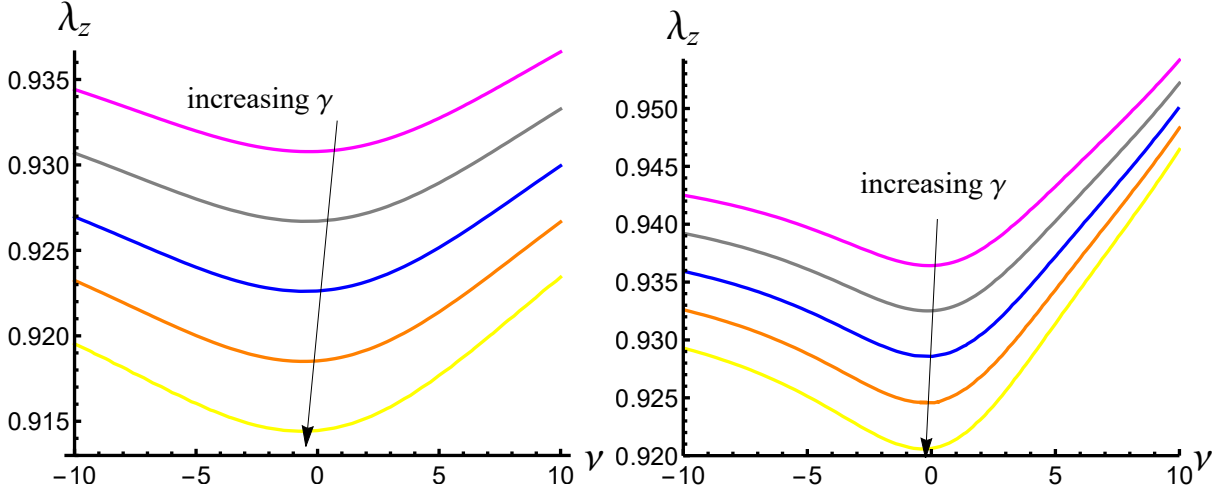


Figure 8: The critical stretch of the buckling mode $m = 1$ as a function of the dimensionless parameter ν with $\kappa = 0.5$ and γ varying from 0.14 to 0.16 with increments of 0.005. The results shown on the left are obtained when $B/A = 1.2$, the ones on the right when $B/A = 1.4$.

effect is amplified. Therefore, the influence of residual stress increases with wall thickness.

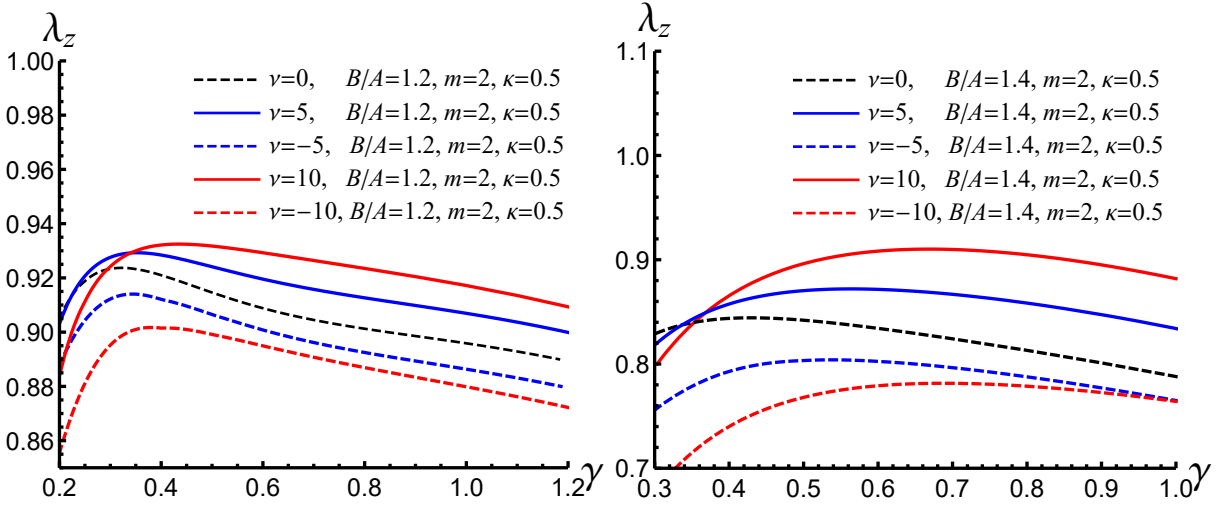


Figure 9: Bifurcation curves for mode $m = 2$, $\kappa = 0.5$ and $\nu = 0, \pm 5, \pm 10$. The results shown on the left are for $B/A = 1.2$, the ones on the right for $B/A = 1.4$.

Phase diagrams are a convenient tool to illustrate mode transitions, which we develop next. Goriely et al. (2008) constructed a phase diagram for a tube with no residual stress and captured the transitions from barreling mode $m = 0$, to Euler buckling $m = 1$ and to mode $m = 2$. Here, in the presence of a residual stress we take $\kappa = 0.5$ to reduce the number of free parameter to three. These are the slenderness ratio γ , the thickness ratio B/A , and the dimensionless residual stress parameter ν . In Figure 11 we illustrate the transitions in the $B/A - \gamma$ plane. The left image illustrates the response with no residual stress, the one on the right when $\nu = 5$. We observe that for low values of B/A higher order modes appear and that an increase in γ amplifies the effect of the residual stress.

Consider, for example, a residually stressed tube with $B/A = 1.05$. Then, the image on the right in Figure 11 shows that for small values of γ the Euler buckling mode $m = 1$ is energetically

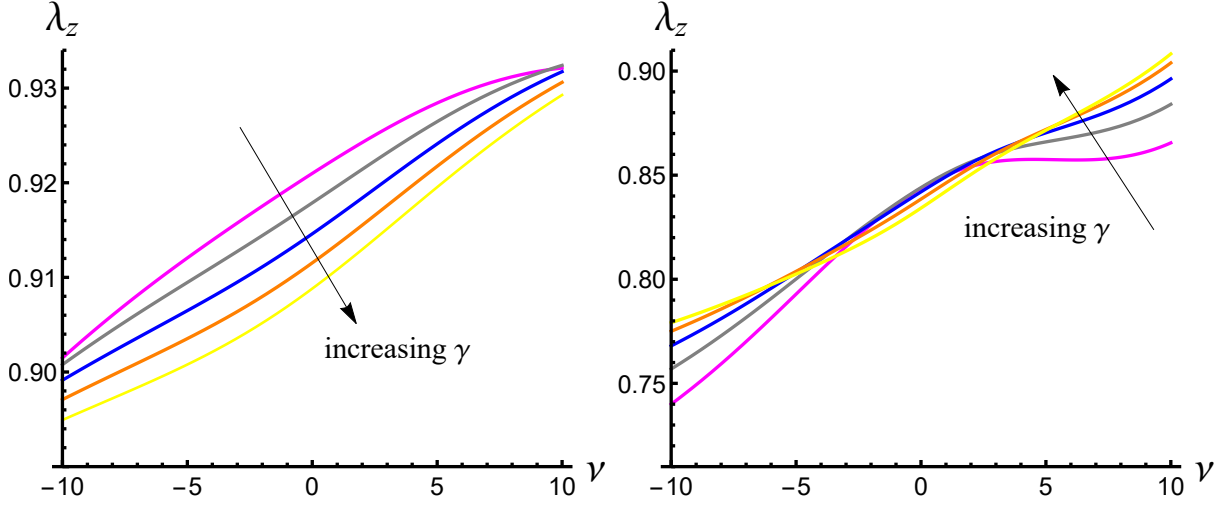


Figure 10: The critical stretch for mode $m = 2$ as a function of the dimensionless residual stress parameter ν , $\kappa = 0.5$ and $0.4 \leq \gamma \leq 0.6$ with increments of $\Delta\gamma = 0.05$. The results shown on the left are for $B/A = 1.2$, the ones on the right for $B/A = 1.4$.

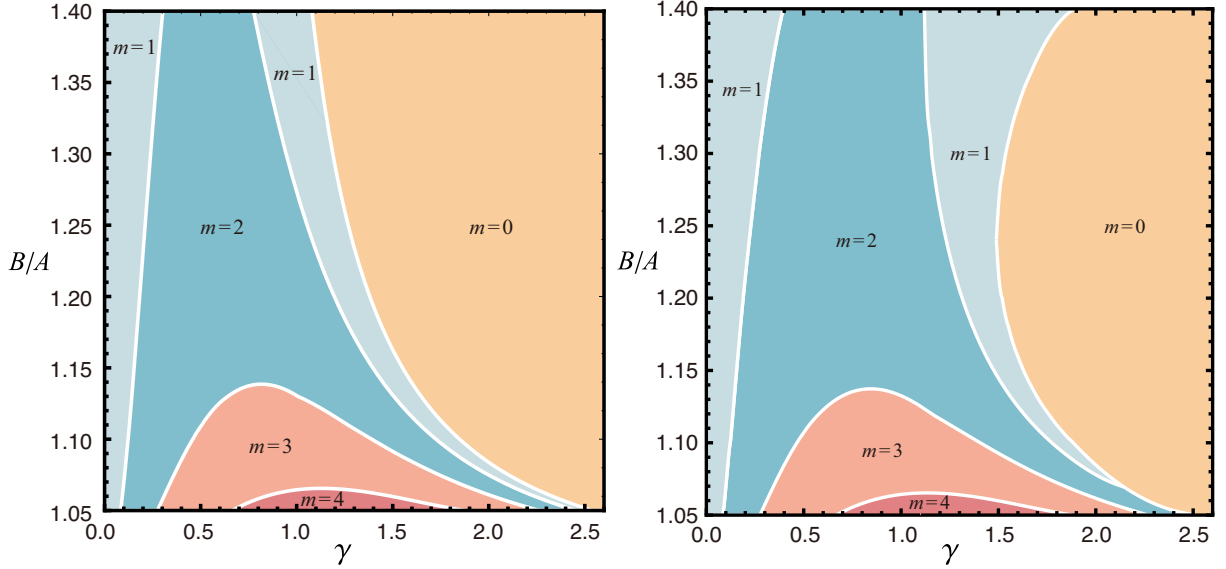


Figure 11: Mode transitions in the $B/A - \gamma$ plane when $\kappa = 0.5$. The left image illustrates the response with no residual stress, the one on the right when the dimensionless residual stress parameter $\nu = 5$.

favorable. With increasing γ , higher order modes emerge and for short tubes with $\gamma > 2.5075$ the barreling mode $m = 0$ dominates. For a tube with $B/A = 1.3$ higher-order buckling modes are absent. We again find that the Euler buckling mode dominates for small values of γ , while for short tubes barreling is preferred.

To provide further insight, we show the bifurcation modes of a compressed tube with no residual stress in Figure 12. It is well known that the linear buckling analysis does not provide the amplitude of the post-buckling states and, for visualization purpose, an arbitrary amplitude is assigned to each mode.

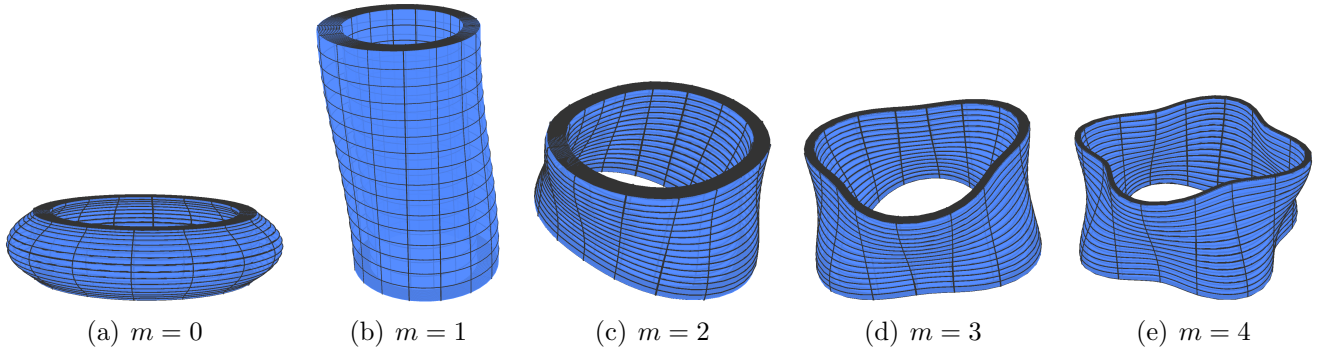


Figure 12: Bifurcation modes for different instabilities. Parameters are: $\gamma = 2$, $B/A = 1.2$ in (a); $\gamma = 1$, $B/A = 1.2$ in (b); $\gamma = 1$, $B/A = 1.1$ in (c); $\gamma = 1$, $B/A = 1.01$ in (d) and $\gamma = 0.3$, $B/A = 1.35$ in (e).

6. Conclusion

In this article we present a detailed stability analysis of a residually stressed tube under compression. The governing equations and boundary conditions are formulated using the theory of nonlinear elasticity, following the works by (Hoger, 1985, 1993, 1996). To obtain explicit results, we specify the radial and circumferential residual stress components for a neo-Hookean material (Sigaeva et al., 2019; Takamizawa, 2022; Zheng and Ren, 2016).

To conduct the buckling analysis, we superimpose an incremental displacement on the primary deformation and deduce an exact bifurcation condition given in Stroh form (Stroh, 1962; Shuvalov, 2003a,b). The buckling analysis is then reduced to studying the linearized increment in the deformation superimposed on a finitely deformed configuration subjected to a residual stress. To evaluate the effect of the residual stress we report the results of a parametric study involving four parameters. These are the wall thickness ratio B/A , the slenderness ratio γ , the dimensionless residual stress and material parameters ν and κ . We determine the critical compression stretch λ_z as a function of the residual stress ν , of the slenderness ratio γ for $B/A = 1.2$ and $B/A = 1.4$ for the stiffness parameter $\kappa = 0.5$ and illustrate the results graphically. Three cases are considered: (i) the barreling mode $m = 0$, the Euler buckling mode $m = 1$ and the mode $m = 2$. Higher order modes such as $m = 3$ emerge in thin-walled tubes only and are therefore only briefly mentioned. In all cases an increase in the wall-thickness amplifies the effect of the residual stress.

We also develop phase diagrams to illustrate transitions from barreling $m = 0$, to Euler buckling $m = 1$ and to mode $m = 2$. Responses with and without residual stress are compared and the results illustrated in the $B/A - \gamma$ plane. We show that for long tubes Euler buckling is energetically favorable, for short tubes the barreling mode dominates.

Acknowledgment

This work was supported by grants from the National Natural Science Foundation of China (Project Nos 12372072, 12072227 and 12021002). Y.L. further acknowledges the UKRI Horizon Europe Guarantee MSCA (Marie Skłodowska-Curie Actions) Postdoctoral Fellowship (EPSRC Grant No. EP/Y030559/1). For the purpose of Open Access, the author has applied a CC BY public copyright license to any Author Accepted Manuscript (AAM) version arising from this submission.

References

- Ahamed, T., Dorfmann, L., Ogden, R. W., 2016. Modelling of residually stressed materials with application to aaa. *Journal of the Mechanical Behavior of Biomedical Materials*, 221–234.
- Brangwynne, C. P., MacKintosh, F. C., Kumar, S., Geisse, N. A., Talbot, J., Mahadevan, L., Parker, K. K., Ingber, D. E., Weitz, D. A., 2006. Microtubules can bear enhanced compressive loads in living cells because of lateral reinforcement. *Journal of Cell Biology* 173 (5), 733–741.
- Bustamante, R., Rajagopal, K. R., Wineman, A., 2024. Residual stresses for a new class of transversely isotropic nonlinear elastic solid. *Mathematics and Mechanics of Solids* 29 (11), 2164–2172.
- Chau, K., 1995. Buckling, barrelling, and surface instabilities of a finite, transversely isotropic circular cylinder. *Quarterly of Applied Mathematics* 53 (2), 225–244.
- Chawla, K., Gupta, A., Bhardwaj, A. S., Thevamaran, R., 2022. Superior mechanical properties by exploiting size-effects and multiscale interactions in hierarchically architected foams. *Extreme Mechanics Letters* 57, 101899.
- Chen, W., Liu, D., Kitipornchai, S., Yang, J., 2017. Bifurcation of pressurized functionally graded elastomeric hollow cylinders. *Composites Part B: Engineering* 109, 259–276.
- Costa, K. D., May-Newman, K., Farr, D., O’Dell, W. G., McCulloch, A. D., Omens, J. H., 1997. Three-dimensional residual strain in midanterior canine left ventricle. *American Journal of Physiology-Heart and Circulatory Physiology* 273 (4), H1968–H1976.
- Dai, H.-H., Wang, F.-F., 2008. Bifurcation to a corner-like formation in a slender nonlinearly elastic cylinder: asymptotic solution and mechanism. *Proceedings of the Royal Society A: Mathematical, Physical and Engineering Sciences* 464 (2094), 1587–1613.
- Dai, H.-H., Wang, F.-F., Wang, J., Xu, J., 2015. Pitchfork and octopus bifurcations in a hyper-elastic tube subjected to compression: Analytical post-bifurcation solutions and imperfection sensitivity. *Mathematics and Mechanics of Solids* 20 (1), 25–52.
- Destrade, M., Ogden, R. W., 2013. On stress-dependent elastic moduli and wave speeds. *IMA Journal of Applied Mathematics* 78 (5), 965–997.
- Dorfmann, A., Haughton, D. M., 2006. Stability and bifurcation of compressed elastic cylindrical tubes. *International Journal of Engineering Science* 44 (18/19), 1353–1365.
- Dorfmann, L., Ogden, R. W., 2021. The effect of residual stress on the stability of a circular cylindrical tube. *Journal of Engineering Mathematics* 127, 1–19.
- Fung, Y. C., 1991. What are the residual stresses doing in our blood vessels? *Annals of Biomedical Engineering* 19, 237–249.
- Fung, Y.-C., 1993. *Biomechanics: Mechanical properties of living tissues*. Springer, Ch. Mechanical properties and active remodeling of blood vessels, pp. 321–391.
- Goriely, A., Vandiver, R., Destrade, M., 2008. Nonlinear euler buckling. *Proceedings of the Royal Society A: Mathematical, Physical and Engineering Sciences* 464 (2099), 3003–3019.

- Haughton, D., Ogden, R., 1979a. Bifurcation of inflated circular cylinders of elastic material under axial loading—I. Membrane theory for thin-walled tubes. *Journal of the Mechanics and Physics of Solids* 27 (3), 179–212.
- Haughton, D., Ogden, R., 1979b. Bifurcation of inflated circular cylinders of elastic material under axial loading—II. Exact theory for thick-walled tubes. *Journal of the Mechanics and Physics of Solids* 27 (5-6), 489–512.
- Hoger, A., 1985. On the residual stress possible in an elastic body with material symmetry. *Archive for Rational Mechanics and Analysis* 88, 271–289.
- Hoger, A., 1993. The constitutive equation for finite deformations of a transversely isotropic hyperelastic material with residual stress. *Journal of Elasticity* 33 (2), 107–118.
- Hoger, A., 1996. The elasticity tensor of a transversely isotropic hyperelastic material with residual stress. *Journal of Elasticity* 42 (2), 115–132.
- Hoger, A., 1997. Virtual configurations and constitutive equations for residually stressed bodies with material symmetry. *Journal of Elasticity* 48, 125–144.
- Holzapfel, G. A., Ogden, R. W., 2010. Modelling the layer-specific three-dimensional residual stresses in arteries, with an application to the human aorta. *Journal of the Royal Society Interface* 7 (46), 787–799.
- Koiter, W. T., 1945. On the stability of elastic equilibrium (in dutch). Ph.D. thesis, Polytechnic Institute of Delft.
- Lan, W.-J., Wang, H.-X., Zhang, X., Chen, S.-S., 2019. Sealing properties and structure optimization of packer rubber under high pressure and high temperature. *Petroleum Science* 16, 632–644.
- Li, T., 2008. A mechanics model of microtubule buckling in living cells. *Journal of Biomechanics* 41 (8), 1722–1729.
- Liu, S. Q., Fung, Y. C., 1989. Relationship between hypertension, hypertrophy, and opening angle of zero-stress state of arteries following aortic constriction. *Journal of Biomechanical Engineering* 111(4), 325–335.
- Liu, Y., 2018. Axial and circumferential buckling of a hyperelastic tube under restricted compression. *International Journal of Non-Linear Mechanics* 98, 145–153.
- Liu, Y., Dorfmann, L., 2024. Localized necking and bulging of finitely deformed residually stressed solid cylinder. *Mathematics and Mechanics of Solids* 29 (6), 1153–1175.
- Liu, Y., Yu, X., Dorfmann, L., 2024. Reduced model and nonlinear analysis of localized instabilities of residually stressed cylinders under axial stretch. *Mathematics and Mechanics of Solids* 29 (9), 1879–1899.
- Melnikov, A., Ogden, R. W., Dorfmann, L., Merodio, J., 2021. Bifurcation analysis of elastic residually-stressed circular cylindrical tubes. *International Journal of Solids and Structures* 226, 111062.

- Merodio, J., Ogden, R. W., 2016. Extension, inflation and torsion of a residually stressed circular cylindrical tube. *Continuum Mechanics and Thermodynamics* 28, 157–174.
- Merodio, J., Ogden, R. W., Rodríguez, J., 2013. The influence of residual stress on finite deformation elastic response. *International Journal of Non-Linear Mechanics* 56, 43–49.
- Norris, A. N., Shuvalov, A., 2010. Wave impedance matrices for cylindrically anisotropic radially inhomogeneous elastic solids. *The Quarterly Journal of Mechanics & Applied Mathematics* 63 (4), 401–435.
- Ogden, R. W., 1997. *Non-linear elastic deformations*. Dover Publications.
- Omens, J. H., Fung, Y.-C., 1990. Residual strain in rat left ventricle. *Circulation Research* 66 (1), 37–45.
- Pan, F., Beatty, M. F., 1997a. Instability of a bell constrained cylindrical tube under end thrust-part 1: Theoretical development. *Mathematics and Mechanics of Solids* 2 (3), 243–273.
- Pan, F., Beatty, M. F., 1997b. Remarks on the instability of an incompressible and isotropic hyperelastic, thick-walled cylindrical tube. *Journal of Elasticity* 48, 218–239.
- Pan, F., Beatty, M. F., 1999. Instability of a bell constrained cylindrical tube under end thrust-part 2: Examples, thin tube analysis. *Mathematics and Mechanics of Solids* 4 (2), 227–250.
- Rajagopal, K., Wineman, A., 2024. Residual stress and material symmetry. *International Journal of Engineering Science* 197, 104013.
- Rausch, M. K., Kuhl, E., 2013. On the effect of prestrain and residual stress in thin biological membranes. *Journal of the Mechanics and Physics of Solids* 61 (9), 1955–1969.
- Shams, M., Destrade, M., Ogden, R. W., 2011. Initial stresses in elastic solids: constitutive laws and acoustoelasticity. *Wave Motion* 48 (7), 552–567.
- Shuvalov, A., 2003a. The frobenius power series solution for cylindrically anisotropic radially inhomogeneous elastic materials. *Quarterly Journal of Mechanics and Applied Mathematics* 56 (3), 327–345.
- Shuvalov, A., 2003b. A sextic formalism for three-dimensional elastodynamics of cylindrically anisotropic radially inhomogeneous materials. *Proceedings of the Royal Society of London. Series A: Mathematical, Physical and Engineering Sciences* 459 (2035), 1611–1639.
- Sigaeva, T., Sommer, G., Holzapfel, G. A., Di Martino, E. S., 2019. Anisotropic residual stresses in arteries. *Journal of the Royal Society Interface* 16 (151), 20190029.
- Sokolis, D. P., 2015. Effects of aneurysm on the directional, regional, and layer distribution of residual strains in ascending thoracic aorta. *Journal of the Mechanical Behavior of Biomedical Materials* 46, 229–243.
- Spencer, A. J. M., 1971. Theory of invariants theory of invariants. in: Eringen, a.c. (ed.). *Continuum Physics*, Academic Press New York 1, 239–353.

- Springhetti, R., Rossetto, G., Bigoni, D., 2023. Buckling of thin-walled cylinders from three dimensional nonlinear elasticity. *Journal of Elasticity* 154 (1), 297–323.
- Stroh, A., 1962. Steady state problems in anisotropic elasticity. *Journal of Mathematics and Physics* 41 (1-4), 77–103.
- Takamizawa, K., 2022. Stretch and stress distributions in the human artery based on two-layer model considering residual stresses. *Biomechanics and Modeling in Mechanobiology* 21 (1), 135–146.
- Vaishnav, R. N., Vossoughi, J., 1987. Residual stress and strain in aortic segments. *Journal of Biomechanics* 20 (3), 235–239.
- Wilkes, E., 1955. On the stability of a circular tube under end thrust. *The Quarterly Journal of Mechanics and Applied Mathematics* 8 (1), 88–100.
- Wolfram, Research, Inc., 2024. Mathematica, Version 14.2. Champaign, IL.
URL <https://www.wolfram.com/mathematica>
- Zheng, X., Ren, J., 2016. Effects of the three-dimensional residual stresses on the mechanical properties of arterial walls. *Journal of Theoretical Biology* 393, 118–126.
- Zhou, Y., Chen, Y., Jin, L., 2023. Three-dimensional postbuckling analysis of thick hyperelastic tubes. *Journal of the Mechanics and Physics of Solids* 173, 105202.
- Zhu, Y., Luo, X., Ogden, R. W., 2008. Asymmetric bifurcations of thick-walled circular cylindrical elastic tubes under axial loading and external pressure. *International Journal of Solids and Structures* 45 (11–12), 3410–3429.